11TH INTERNATIONAL SYMPOSIUM ON FLOW VISUALIZATION
August 9-12, 2004, University of Notre Dame, Notre Dame, Indiana, USA

VISUALIZING INDEX-OF-REFRACTION VARIATIONS IN OPTICALLY ACTIVE FLOW FIELDS

Daniel Duffin*, Stanislav Gordeyev, Eric Jumper*****
*** University of Notre Dame, 118 Hessert Laboratory, Notre Dame, IN 46556-5684 USA**
**** University of Notre Dame, 121 Hessert Laboratory, Notre Dame, IN 46556-5684 USA**
***** University of Notre Dame, 110 Hessert Laboratory, Notre Dame, IN 46556-5684 USA**

Keywords: *wavefront sensors, optical aberrations, shear-layer structures, index-of-refraction, tomography*

ABSTRACT

Light passing through an optically active flow field becomes distorted due to index-of-refraction variations in the flow field. In many cases these index-of-refraction variations are caused by density or temperature variations in the flow. These variations cause an otherwise-planar optical wavefront to be imprinted with time-varying aberrations. Optical aberrations are commonly measured by their optical path difference (OPD), which is the mean-removed integral of the index-of-refraction field along the path the light beam takes through the flow field. By using geometric optics and Taylor's frozen flow approximation the OPD can be measured directly from the deflection angle of the light beam as it exits the flow field. Using this simple technique one can obtain a time history of OPD, which can then be extrapolated into a one-dimensional map of the flow's OPD field. This map can be interpreted to reveal much information about the flow field and the structures contained in the flow. For example, the slope of the space-time streaks in the map is the convection velocity of the structures in the flow. The evolution of the maps also divulges how the flow's structures are evolving, revealing vortex pairing, for example. The amplitude of the OPD can indicate the strength of mixing in the flow. This simple yet unconventional flow visualization technique can reveal a plethora of information about turbulent flows not available by other means.

1 INTRODUCTION TO AERO-OPTIC INTERACTIONS

The purpose of this paper is to briefly review the use of wavefront sensors of various designs to visualize index-of-refraction variations in turbulent flows. While these sensors can be used for liquid flows, this paper will discuss only gas applications due to the simple linear relationship between a gas's density and its index-of-refraction. The fact that a medium's index-of-refraction is defined as the speed of light in a vacuum divided by the speed of light in the medium has long been exploited in the visualization of flows. In most cases of interest to the flow-visualization community, diffraction effects are second order and ray-tracing or geometric-optic theory sufficiently describes the function of both the more-traditional optical flow-visualization techniques and the wavefront sensing techniques to be discussed here. Geometric optics is based on Huygens' Principle [1], which finds its origin in physical optics. Consider a planar wavefront (i.e., a perfectly collimated beam of monochromatic light) encountering a region of variable-index flow, as depicted in Fig. 1. As the light propagates through the region, due to the differences in the speed of light in

the medium, the previously planar wavefront will emerge advanced and retarded from its mean location; such a distorted wavefront is referred to as aberrated. Huygens' Principle states that as the wavefront emerges, each portion of the wavefront will travel in the direction of its local normal (i.e., in a direction normal to itself) [1,2]; this is indicated in Fig. 1 as the greatly-exaggerated direction vectors above the aberrated wavefront. In fact, if a small-diameter (small-aperture) laser beam, originally normal to the lower (planar) wavefront, were to propagate through the same medium, it would emerge normal to the aberrated wavefront at that location, like one of the direction vectors themselves.

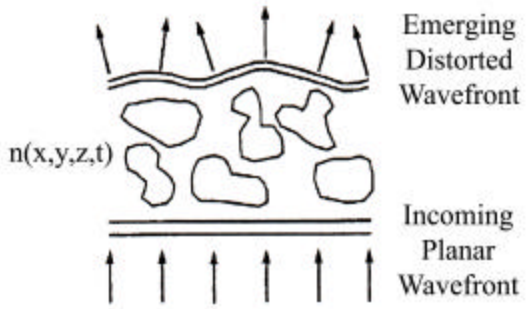

Fig. 1 - Planar wavefront distorted by index-of-refraction variations in the flow field. [1, 2]

In recent years the engineering significance of the aberrating effect of turbulent flows on large-aperture laser beams has become extremely important. While it is not the purpose of this paper to dwell on the engineering significance, it is worth stating this significance, because it is this engineering application that has led to the rapid advance in wavefront sensing technology over the last decade. When the cause of the variable-index medium is a turbulent flow, Fig. 1 would represent the aberrated wavefront at a single instant in time. In fact, as indicated in Fig. 2, the aberrating structures in a turbulent flow convect and evolve with the flow; in this case, the figure depicts a heated two-dimensional (planar) jet undergoing Kelvin-Helmholtz instabilities, becoming turbulent and mixing with the ambient, lower-temperature and thus higher-index-of-refraction air.

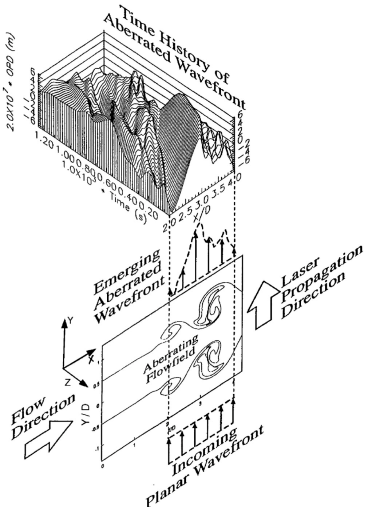

Fig. 2 - Time history of aberrated wavefronts. [3,4]

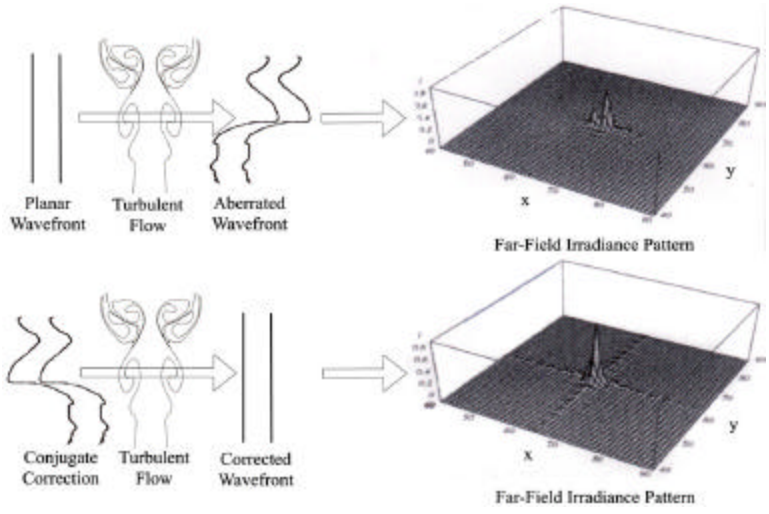

Fig. 3 - Adaptive-optic correction theory and corresponding far-field intensity patterns. [4]

Figure 2 also shows a time series of instantaneous aberrated wavefronts due to the propagation of an otherwise-planar wavefront through the jet [3,4]. This figure illustrates an important characteristic of these, so-called *aero-optic*, turbulent-flow-induced aberrations: they are highly time-varying. The aberrated wavefronts are near-field optical effects; their significance, however, is their effect in the far-field. There are a number of airborne laser systems being developed today whose performance depends on the ability to focus large-aperture lasers on distant targets in the far-field; these aberrated wavefronts degrade the beam's focus or on-axis intensity from its perfect 'diffraction-limited' intensity. Fig. 3 depicts an instantaneous degraded focus for the first wavefront from Fig. 2 [4]. If a conjugate to the aberration that the turbulence would produce is impressed on the beam prior to its propagation through the turbulent region, a planar wavefront would emerge from the turbulent region and restore diffraction-limited performance; this is depicted in the lower portion of Fig. 3 [4]. In order to impose the conjugate, the aberrating quality of the turbulence must be sensed (with a wavefront sensor), a conjugate constructed and applied to a deformable mirror, and the beam reflected from the mirror prior to it propagation through the aberrating flow field; systems that perform this process are called adaptive-optic systems [5]. In real flight scenarios, this process must take place at upwards of 10-20 kHz, requiring wavefront sensors that operate in real time at upwards of 100 kHz. Such systems are not yet achievable, but at Notre Dame instruments that capture wavefronts (for post processing) at rates in excess of 100 kHz have been developed [6]. These instruments have allowed us to study turbulence in new ways and have, in fact, led to the discovery of new fluid-mechanic mechanisms at work in creating index variations in high-speed flows [2,7,8].

Wavefronts are usually quantified using a related quantitative measure, the optical path difference (OPD), which is the mean-removed optical path length (OPL). OPL is defined as the path-integral of the index-of-refraction field along the path of the beam,

$$OPL(x,z,t) = \int_{s_1}^{s_2} n(x,y,z,t)\,ds. \tag{1}$$

Where s_1 and s_2 are the entrance and exit positions, respectively, along the path the beam takes through the flow field [1, 2]. OPD is obtained by removing the mean OPL over the aperture,

$$OPD(x,z,t) = OPL(x,z,t) - \overline{OPL}(t). \tag{2}$$

2 OPTICAL FLOW-VISUALIZATION TECHNIQUES

2.1 Traditional Techniques

As mentioned earlier, optical methods of quantifying OPD for the purpose of flow visualization have long been used in fluid mechanics. An excellent review of these methods can be found in Reference 9. The simplest method to implement is the shadowgraph; it works on the principle that an otherwise collimated large-aperture beam of light refracts as it propagates through a flow field with index-of-refraction gradients. Thus the emerging light, when viewed on a screen, will show bright areas where light rays converge and dark areas where light rays diverge. Almost always used as a qualitative technique, shadowgraphs record the path-integral of the second derivative of the index-of-refraction along the direction normal to the light propagation.

A Schlieren system is another common technique used to capture or visualize the path-integrated index-of-refraction field. As in the case of the shadowgraph, an otherwise-collimated, large-aperture beam is propagated through the index field, but in this case, the light exiting the flow field is passed through a lens and passed by a knife edge located at the focal point of the lens. The knife edge "filters" (clips) the light rays that are refracted towards the knife edge. Again, used primarily as a qualitative instrument, the Schlieren measures the first derivative of the index-of-refraction in the direction normal to the light propagation.

A third commonly used technique is interferometry. In this technique, the OPD of the aberrated beam is directly captured by comparing the beam's wavefront after propagation through the medium with a wavefront unaberrated by the medium. This comparison is made by interfering the two large-aperture, otherwise-collimated, monochromatic light beams and observing (photographically capturing) the fringe pattern due to the interference of the two beams [9]. By analyzing the fringe shift from a control-case exposure and a flow-case exposure one can infer the OPD(x,y) over the aperture. Although interferograms can be extremely accurate by improvements incorporating lasers and holography, for example, their capture rates are well below 100 Hz.

2.2 Wavefront Techniques

Because of the advance in the design and availability of wavefront sensors, their use in flow visualization is beginning to develop. The first so-called wavefront sensors were, in fact, interferometers. However, because of the tedious nature of their data reduction, other methods have been developed to more-directly measure wavefronts. One of the first wavefront sensors to be developed was the Hartmann wavefront sensor [2]. The Hartmann sensor makes use of Huygens' Principle and directly measures the spatial derivative of the wavefront at discrete locations over the aperture. A schematic of an early Hartmann sensor (or Hartmann plate, as it was initially referred to) is shown in Fig. 4.

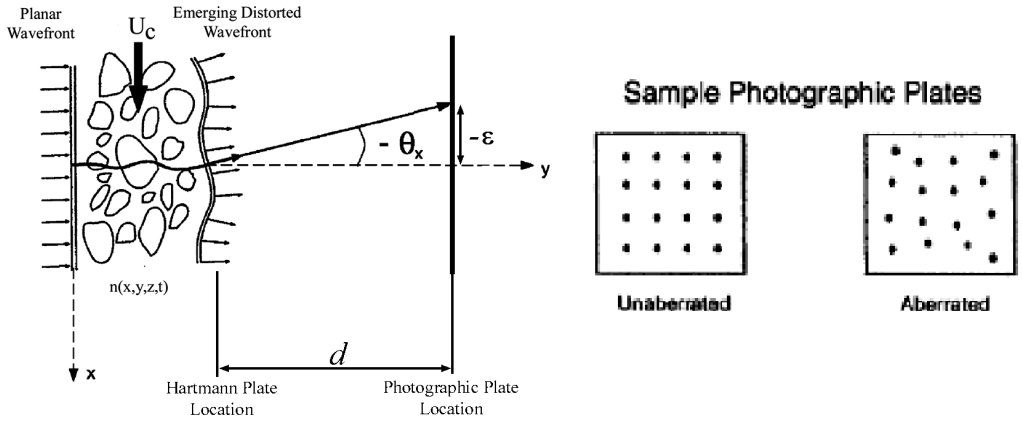

Fig. 4 – Planar wavefront distorted by optically active flow field and samples of resulting Hartmann plate dot displacements. [2]

The way the sensor is implemented is by placing an opaque screen at the location where the light beam exits the flow field. This opaque screen has an array of small holes which allow light to pass through at those discrete points. When there are no disturbances in the flow (the unaberrated case), the light rays pass through the holes and strike a photographic plate placed at a known distance, d,

from the Hartmann plate. Once exposed, an array of dots is recorded on the photographic plate to form a fiducial grid. When passed through the aberrating flow these light rays move from their unaberrated positions by a small distance, ε. By re-exposing the photographic plate, a second set of dots are recorded on the plate. Knowing the new locations, and thus the displacements in the plane of the photographic plate, and the distance to the plate, the displacement angles, $?_{x,y}$, can be found. As given by Huygens' Principle, the tangents of these instantaneous angles are the spatial derivatives of the wavefront. If we consider only the derivatives in the flow direction, x-direction, a wavefront can be constructed [2] by integrating the slopes,

$$OPL(t,x) = \int_o^x \left(\frac{\mathrm{d}OPL}{\mathrm{dx}} \right) \mathrm{dx} = \int_o^x (q_x)\mathrm{dx}. \tag{3}$$

Since $?_x$, is known at discrete locations, the accuracy of the wavefront depends on the integration scheme and how accurately the discrete slopes represent the average slope between holes.

The first improvement on the basic Hartmann sensor was the replacement of the Hartmann plate with a lenslet array. Shack [10] determined that the addition of the lenslet array increases the sensor's accuracy because the deflection angle through the lenslet represents the average wavefront slope over the entire sub-aperture of the lenslet, not just one small hole's location. The improved sensor is known as a Shack-Hartmann wavefront sensor and is in common use today with the photographic plate replaced by a CCD array. The CCD array allows for the collection of large numbers of wavefronts; however, except in the case of very-low-speed flows, each wavefront is time uncorrelated to its neighbor because of the limited framing rate dictated by the combined frame grabber and CCD camera. Typical framing rates range from 15 Hz on the lowest end to 1 – 2 kHz for state-of-the-art CCD systems. One-Dimensional CCD arrays (referred to as line-scan cameras) typically operate at framing rates up to ~ 2 kHz. An interesting example of the use of a one-dimensional Shack-Hartmann sensor using a line-scan camera for visualization of the temperature/density field in an axisymetric heated jet was carried out by researchers at the Air Force Research Laboratory (AFRL) Phillips site [2]. They used eight one-dimensional Shack-Hartmann sensors placed radially around the jet, to capture simultaneous one-dimensional, cross-stream wavefronts from eight views through the jet, see Fig. 5. Since each wavefront represents a integrated slice through the flow field, tomographic-reconstruction routines developed for use in X-radiography were used to construct two-dimensional slices through the jet; these slices were then stacked in time to visualize the time evolving scalar temperature field, shown in Fig. 6.

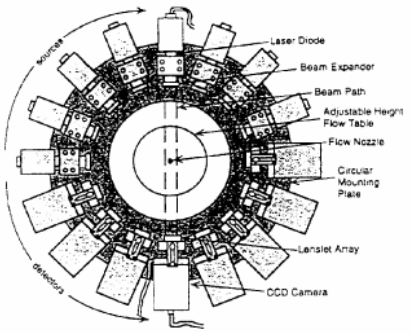

Fig. 5 – Schematic of Shack-Hartmann setup on the axisymmetric jet at AFRL. [2]

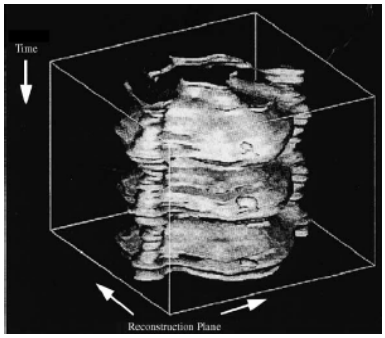

Fig. 6 – Reconstruction of the temperature field of the axisymmetric jet at AFRL. [2]

To capture the time evolution of aberrated wavefronts due to propagation through turbulent flows of practical interest to airborne optical platforms, frame rates of 20 – 100 kHz are needed; these rates are not available from CCD cameras. Malley et al. [11] were the first to recognize the fact that aberrations on a wavefront due to flow structures convecting in the flow must themselves convect, see Fig. 2. This fact was the key that allowed pseudo wavefronts to be constructed with a single sensor. By capturing a running time series of wavefront slopes at the single probe-beam location, Malley et al. traded integration in space, equation (3), for integration in time using *a priori* knowledge of the convection velocity, U_c, of the aberrating structures in the flow. Thus, a running time series of slopes could be converted into a time series of OPL at the probe position, $\bar{x}$, as,

$$OPL(t,\bar{x}) = \int_{t_o}^{t}\left(\frac{\mathrm{d}OPL(t,\bar{x})}{\mathrm{dx}}\right)\frac{\mathrm{dx}}{\mathrm{d}t}\,\mathrm{d}t = \int_{t_o}^{t} -q_x(t,\bar{x})U_c\,\mathrm{d}t. \tag{4}$$

This OPL could then be 'propagated' forward and aft of the measurement location to create pseudo one-dimensional wavefronts in the flow direction using Taylor's frozen-flow hypothesis by trading time and position, again, through knowledge of U_c. The main problem in this original technique is determining the convection velocity, U_c. Over the last few years Notre Dame has developed a new derivative instrument we refer to as a *Malley Probe* [12], which directly measures U_c, by adding a second, closely-spaced probe beam; this new instrument is shown schematically in Fig. 7. Since the beams are closely spaced, the aberrations in the fluid convect with the flow remaining essentially unchanged; the displacement signals from the two position sensing devices are then essentially the same except one is shifted in time from the other. Performing a cross-correlation of the two signals reveals this time shift, t. The convection velocity can then be calculated from the known spacing between the two probe beams, ?:

$$U_c = \frac{\Delta}{t}. \tag{5}$$

With this technique, one has the ability to make time-resolved measurements of OPL at one location in the flow, produce pseudo wavefronts over selectable aperture sizes, extract aberration scale sizes, construct OPD as a function of aperture size and determine aberration convection velocities.

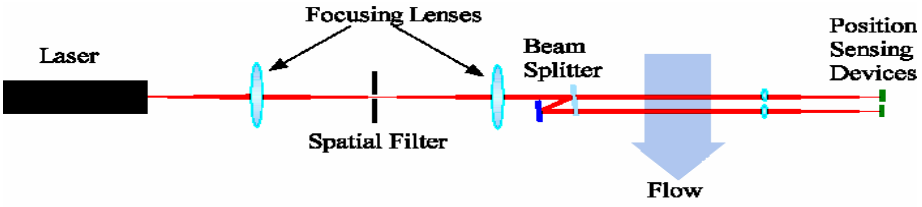

Fig. 7 – Schematic of a Notre Dame Malley Probe.

Another Malley-related instrument, the Small Aperture Beam Technique (SABT), was also developed at Notre Dame [3]. The SABT makes use of multiple probe beams placed along the flow direction to capture time histories of off-axis beam displacements at a number of locations a finite distance apart in the flow direction over a relatively large aperture. The changes in the characteristic of one displacement signal to the next captures the evolving nature of the aberrating flow structures. The multiple probe beams are used to both determine the convection velocity as a function of position over the aperture and, through a weighed average, to reconstruct highly-accurate OPD at locations in-between the probe beams. This technique allows for both the spatial and temporal

reconstruction of the flow field's wavefront with a sparse number of sensors. The Malley Probe and the SABT sensor offer two powerful techniques for making time-resolved, quantitative measurements of the optical aberrations in a flow field via construction of OPD maps, as in Fig. 2, at capture rates in excess of 100 kHz.

3 USING WAVEFRONT SENSING TO 'VISUALIZE' VORTEX ROLL-UP AND PAIRING

A number of uses of wavefront sensors for studying fluid mechanics can be found in Reference 2; however, to demonstrate the potential of using wavefront sensors to 'visualize' and study fluid mechanic processes in ways not available by other means, a recent example of our use of these sensors to study the formation and evolution of vortical structures in shear layers is presented here. This study used the two-dimensional heated jet facility (2DHJ) located in the Aero-Optics Lab at the University of Notre Dame's Hessert Laboratory for Aerospace Research. Although recently reconditioned, the basic facility is described in detail elsewhere [3,4]. A photograph and schematic of the of the facility is shown in Fig. 8. The jet is fed by air heated approximately 55°C above ambient room temperature through a two-dimensional, 16:1 contraction nozzle with an exit width, D, of 1.27 cm. The jet's core velocity is 7 m/s. The coherent structures that form in the two shear layers at the edges of the jet convect at approximately 3.5 m/s.

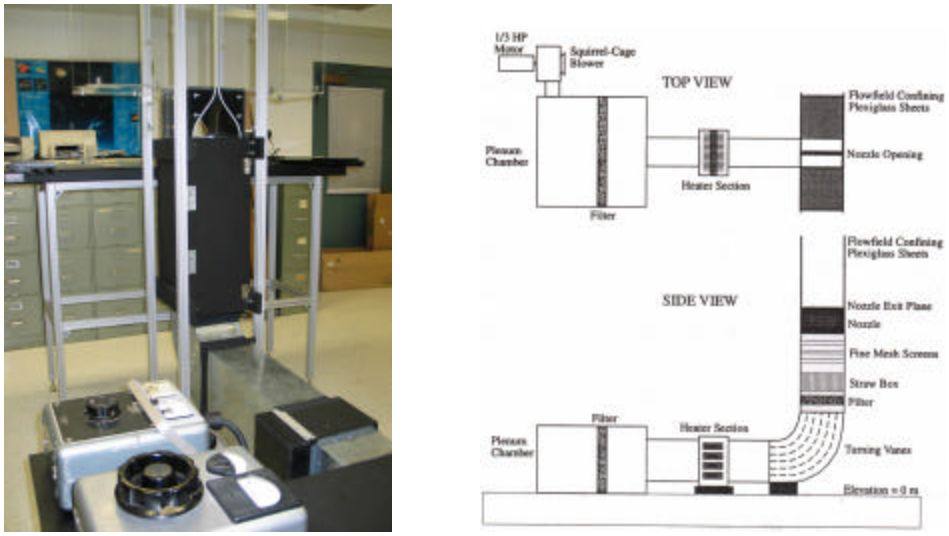

Fig. 8 - The two-dimensional heated jet facility at the University of Notre Dame's Hessert Laboratory for Aerospace Research.

The temperature variations in the jet cause density variations, ρ', and these, in turn, create index-of-refraction variations, n', through Gladstone-Dale relationship,

$$n' = K_{GD}\,\rho', \tag{6}$$

where K_{GD} is the Gladstone-Dale constant. As will be shown, capturing these index variations allows one to quantitatively and visually study the vortical structure formation in the shear layers under the influence of the Kelvin-Helmholtz instability with and without forcing, in this case acoustic forcing. The acoustic forcing was achieved by placing a single speaker perpendicular to the

jet's core flow in jet's exit plane and at a distance of approximately one meter from the jet. The speaker was driven by an amplifier whose input was a selectable sine wave from a function generator.

3.1 Effects of Acoustic Forcing

Figures 9 (a) and (b), captured using an SABT sensor, show the effect that acoustic forcing had on the jet. When there was no forcing the jet's wavefront (OPD) pattern, Fig. 9 (a), is seen to have a center temporal/spatial frequency around which aberrating vortical structures form in random patterns within some standard deviation. When acoustically forced (in this case at ~ 240 Hz), Fig. 9 (b), one can see that the wavefront pattern becomes periodic and 'regularized.' Careful examination of Fig. 9 (b) reveals that the larger structures are at the sub-harmonic, 120 Hz, and the 240 Hz pattern is present only in the most upstream location ($2.0 < X/D < 2.5$) suggesting that the acoustic control is regularizing the first-unstable-mode roll-up and the second mode (vortex pairing) is, in turn, organized by the initial roll-up event. When forced at the sub-harmonic, ~ 120 Hz, the jet was again regularized, but in this case through control of the second mode.

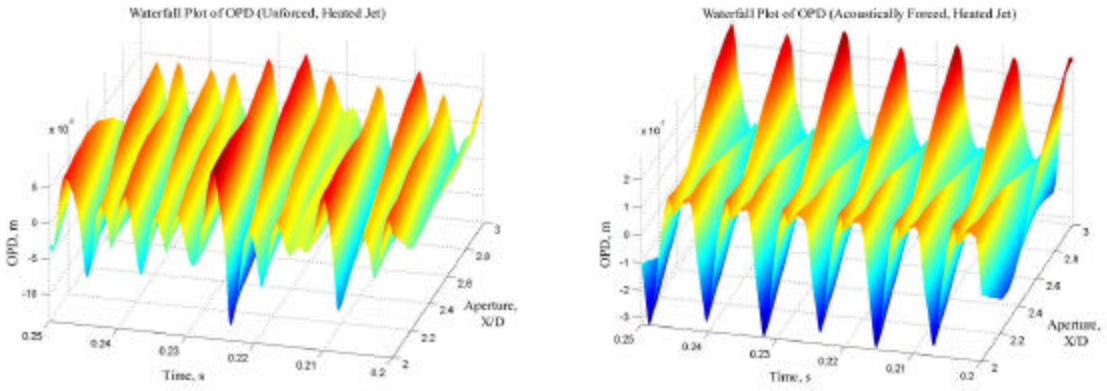

(a) (b)

Fig. 9 - Wavefront characterizations of the two-dimensional heated jet: (a) Unforced case, (b) Acoustically forced case.

One should note that the slope of the space-time streaks in the OPD pattern, being a position-time map, gives the convection velocity of the aberrating structures. Further, the coherence lengths of the patterns directly reveals the vortical structure sizes, and the p-v amplitude of the OPD can be used to infer the mixing taking place in the shear-layer. Clearly, the use of wavefront sensors to explore this flow reveals a plethora of information from a single source that is not available from other instruments in common use in fluid mechanics.

3.2 Comparison of a Malley Probe with a Two-Dimensional Wavefront Sensor

Although the previous data were obtained using an SABT sensor, it is interesting to examine just how much information can be obtained with a single Malley Probe. Recall that the Malley Probe gathers wavefront-slope information at a single location and extrapolates this information upstream and downstream from its probe beam location assuming the flow is frozen. Recently we had an opportunity to compare Malley-Probe-extrapolated time series of wavefronts for the acoustically-forced heated jet with those collected from a *Phase-Diversity*-type wavefront sensor. In this case, a time series of one-dimensional strips at the Malley Probe location was extracted from the two-

dimensional wavefronts and compared to the Malley Probe results; the results are shown in Fig. 10, which is a time series of one-dimensional wavefronts, as in Fig. 9, but looking down into the time-position plane. Figure 10 shows that the size, shape, and position of the aberrations on the wavefronts are quite similar. The slopes of the light/dark (or red/blue) streaks in the maps show the convection velocity of the structures. Both sensors show that the structures are passing at about 3.5 m/s. Also, the spacing between the light/dark streaks shows that the passing frequencies of the structures captured by the two sensors are the same. The passing frequency of the largest structures is ~ 120 Hz. Beyond these two obvious similarities one can also see similarities in the small scale structures in the flow. The obvious difference in the two is the lack of crispness in the two-dimensional wavefront sensor due to its relatively-slow framing rate, ~ 500 Hz, and its spatial resolution. All the relevant information for a fluid-mechanic study is present in the Malley-Probe results.

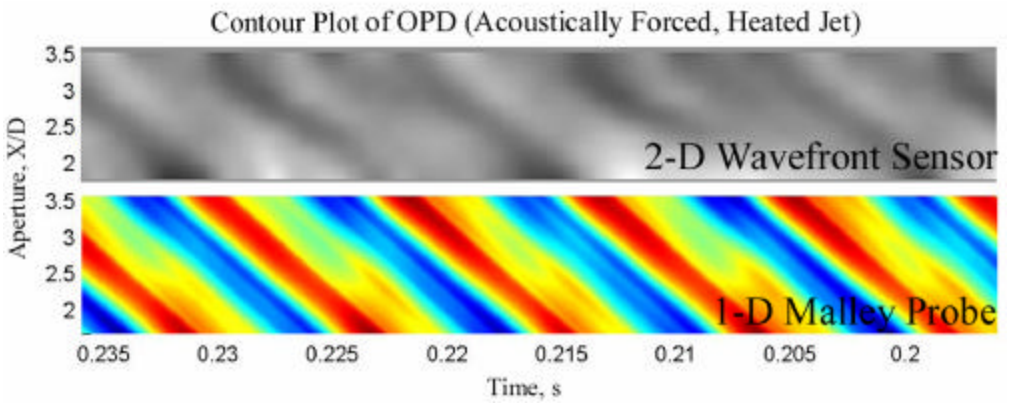

Fig. 10 - Comparison of wavefront measurements from a 2-D wavefront sensor and a 1-D Malley Probe.

3.3 Forcing Characterization

In an attempt to explore the locking character of the jet's fundamental and sub-harmonic modes, the jet was acoustically forced and Malley Probes were positioned at sixteen locations in the streamwise direction, ranging from $1.0 < X/D < 4.0$. At each location, the time series were phase-locked averaged over two cycles of the 120 Hz forcing. In each case, the mean was removed so that the time series of phase-locked OPD at each of the probe-beam locations could be patched together with the other locations. This data set was instructive in understanding the effect that the forcing was having on the formation and pairing of the vortical structures. Figures 11 (a) and (b), show phase plots of OPD(f ,x) (phase being directly related to time) at two locations in the flow representing a location where only the first vortical structure roll-up is present ($X/D = 1.4$) and a location downstream of where paring of the structures has taken place ($X/D = 3.4$).

Splicing all the Malley Probe data together led to the 'surface' map shown in Fig. 12. The method of reducing and splicing the data together resulted in a somewhat choppy plot, but it is never-the-less instructional. The interesting portion of these figures is the region from $2.0 < X/D < 2.5$, where it can be seen that structures with a frequency of 240 Hz start to disappear and structures with a frequency of 120 Hz start to appear. Clearly, the wavefronts are capturing and 'visualizing' the vortex pairing events, now regularized by the forcing.

The black lines on Fig. 12 (b) are drawn to emphasize the trends of the peaks in the OPD signal. The dashed lines represent the initial roll-up of the vortices, which are passing at 240 Hz. At

a location around X/D = 2.5, these 240 Hz vortices pair and turn into vortices passing at 120 Hz. The 120 Hz vortices are noted with the solid black lines in Fig. 12 (b). In the near future, we will be exploring forcing at both the fundamental and sub-harmonic with different phase shift between them in an attempt to control the location where this pairing occurs.

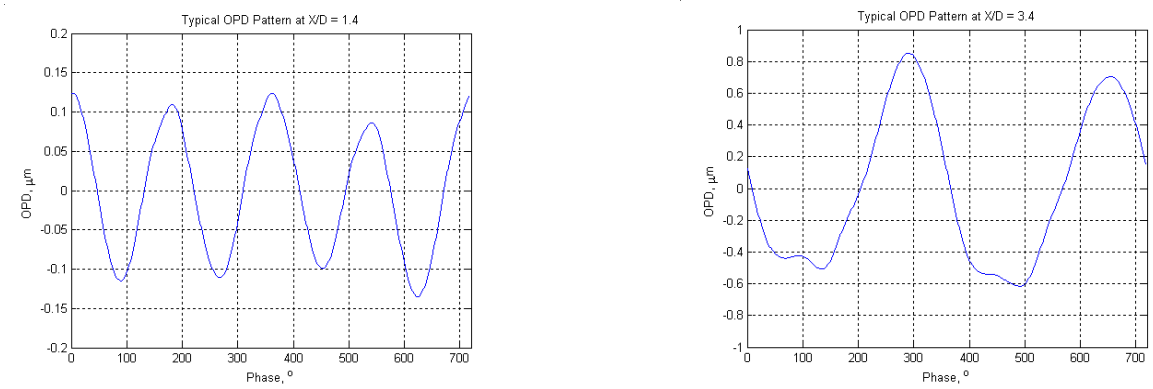

(a) (b)

Fig. 11 – Typical OPD patterns: (a) X/D = 1.4, (b) X/D = 3.4.

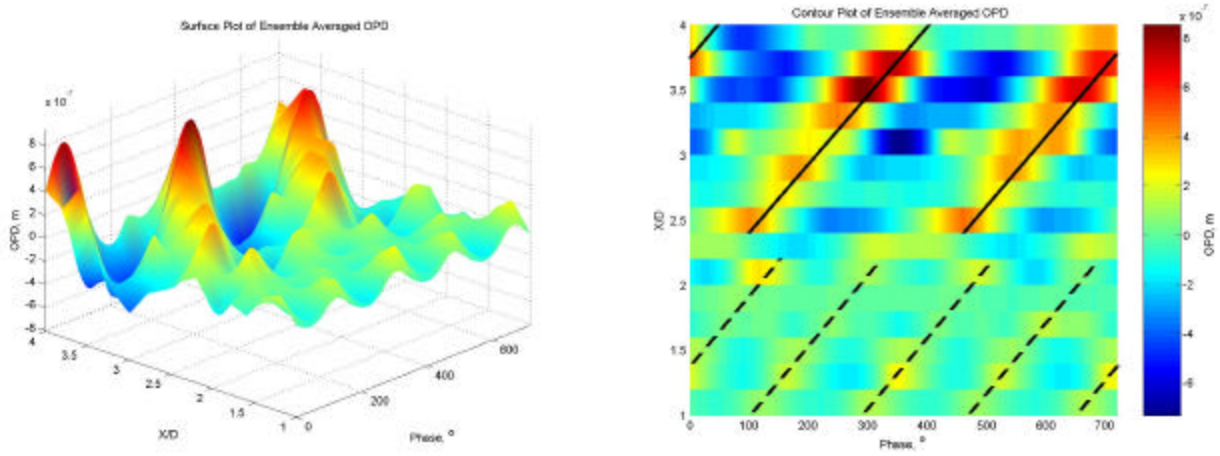

(a) (b)

Fig. 12 – Wavefront (OPD) measurements from the vortex pairing experiment:
(a) Surface plot of OPD, (b) Contour plot of OPD.

4 CONCLUSIONS

The recent advance of wavefront sensing technology in the last decade has now led to a wide range of instruments that are useful to the experimental fluid mechanics community. As we speak, a reasonably-priced commercial Malley Probe package with user-friendly software is about to hit the market [13]. This paper has really only scratched the surface of what can be learned using this new technology. Its utility in mixing and combustion studies, for example, has not even been touched on. Our hope is that this paper encourages others to explore ways that this technology might aid you in your research.

REFERENCES

1. Klein M. *Optics*. Wiley, 1970.
2. Jumper E and Fitzgerald E. Recent Advances in Aero-Optics. *Progress in Aerospace Sciences*, Vol. 37(2001), pp 299-339, 2001.
3. Hugo R and Jumper E. Experimental Measurement of a Time-Varying Optical Path Difference by the Small-Aperture Beam Technique. *Applied Optics*, Vol. 35(22), pp. 4436-4447, 1996.
4. Cicchiello J and Jumper E. Far-Field Optical Degradation due to Near-Field Transmission through a Turbulent Heated Jet. *Applied Optics*, Vol. 36(25), pp. 6441-6452, 1997.
5. Tyson R. Adaptive-Optics Engineering Handbook. *Optical Engineering Series*, Vol. 67, pp 1-25, 2000.
6. Jumper E and Hugo R. Quantification of Aero-Optical Phase Distortion Using the Small-Aperture Beam Technique. *AIAA Journal*, Vol. 33(11), pp 2151-2157, 1995.
7. Hugo R, Jumper E, Havener G and Stepanek S. Time-Resolved Wave Front Measurements through a Compressible Free Shear Layer. *AIAA Journal*, Vol 35, pp. 671-677, 1997.
8. Fitzgerald E and Jumper E. The Optical Distortion Mechanism in a Nearly Incompressible Free Shear Layer. *Journal of Fluid Mechanics*, 2004.
9. Goldstein R. *Fluid Mechanics Measurements*. Hemisphere, 1983.
10. Malacara D. *Optical Shop Testing*. Wiley, 1978.
11. Malley M, Sutton G and Kincheloe N. Beam-Jitter Measurements of Turbulent Aero-Optical Path Difference. *Applied Optics*, Vol. 31, pp. 4440-4443, 1992.
12. Gordeyev S, Jumper E, Ng T and Cain A. Aero-Optical Characterization of Compressible, Subsonic Turbulent Boundary Layers. *AIAA Paper* 2003-3606, June 2003.
13. Contact ITAC through Cain A. P.O. Box 6971, Chesterfield, MO 63006, USA.